

Radiative dileptonic decays of B-meson in the general two Higgs doublet model

G. ERKOL AND G. TURAN

Physics Department, Middle East Technical University, 06531, Ankara, Turkey

E-mail: gurerk@newton.physics.metu.edu.tr

E-mail: gsevgur@metu.edu.tr

We investigate the exclusive $B \rightarrow \gamma \ell^+ \ell^-$ decay in the general two Higgs doublet model (model III) including the neutral Higgs boson effects with an emphasis on possible CP-violating effects. For this decay, we analyse the dependences of the forward-backward asymmetry of the lepton pair, A_{FB} , CP-violating asymmetry, A_{CP} , and the CP-violating asymmetry in forward-backward asymmetry, $A_{CP}(A_{FB})$, on the model parameters and also on the neutral Higgs boson effects. We have found that $A_{FB} \sim 10^{-1}, 10^{-2}$, $A_{CP} \sim 10^{-2}, 10^{-1}$ and $A_{CP}(A_{FB}) \sim 10^{-2}, 10^{-1}$ depending on the relative magnitude of the Yukawa couplings $\xi_{N,tt}^U$ and $\xi_{N,bb}^D$ in the model III. We also observe that these physical quantities are sensitive to the model parameters and neutral Higgs boson effects are quite sizable for some values of the coupling $\xi_{N,\tau\tau}^D$.

PACS number(s): 12.60.Fr, 13.20.He

1. Introduction

It has been realized for a long time that rare B-meson decays induced by the flavor-changing neutral currents (FCNC) are the most promising field for obtaining information about the fundamental parameters of the standard model (SM), like the elements of the Cabibbo–Kobayashi–Maskawa (CKM) matrix, the leptonic decay constants etc., and testing the SM predictions at loop level. At the same time rare decays can also serve as a good probe for establishing new physics beyond the SM, such as the two Higgs doublet model (2HDM), minimal supersymmetric extension of the SM (MSSM) [1], etc., since the contributions from these new models and the SM arise at the same order in perturbation theory. The observation of radiative penguin mediated processes, in both the exclusive $B \rightarrow K^* \gamma$ [2] and inclusive $B \rightarrow X_s \gamma$ [3] channels, stimulated the investigation of the radiative rare B meson decays with a new momentum. Among these rare decays, $B \rightarrow \gamma \ell^+ \ell^-$ ($\ell = e, \mu, \tau$) have received a special interest due to their relative cleanliness and sensitivity to new physics. They have been investigated in the framework of the

SM for light and heavy lepton modes in refs.[4]-[6]. The new physics effects in these decays have also been studied in some models, like MSSM [7] and the two Higgs doublet model [8, 9, 10].

In this work, we study the radiative $B \rightarrow \gamma \ell^+ \ell^-$ decay in the general two-Higgs doublet model (model III) including the neutral Higgs effects. The 2HDM is the minimal extension of the SM, which consists of adding a second doublet to the Higgs sector. In this model, the Yukawa Lagrangian responsible for the interaction of quarks and leptons with gauge bosons opens up the possibility of having tree-level FCNC, which are forbidden in the SM and model I and II types of the 2HDM. This brings new parameters, i.e., Yukawa couplings, into the theory.

$B \rightarrow \gamma \ell^+ \ell^-$ decay is induced by the pure-leptonic decay $B \rightarrow \ell^+ \ell^-$, which is free from the helicity suppression, in contrast to the channels with light leptons, but quite hard to detect experimentally due to low efficiency. In $B \rightarrow \gamma \ell^+ \ell^-$ decay, helicity suppression is overcome by the photon emission in addition to the lepton pair. For this reason, it is expected for $B \rightarrow \gamma \ell^+ \ell^-$ decay to have a large branching ratio and this makes its investigation interesting. Another reason that motivates to study $B \rightarrow \gamma \ell^+ \ell^-$ process is that it receives additional contributions from the neutral Higgs boson (NHB) exchanges in the 2HDM. Since NHB contributions are proportional to either the lepton mass or the corresponding Yukawa coupling, they are negligible for $B \rightarrow \gamma \ell^+ \ell^-$ decays with light leptons, but we could expect significant contributions for $\ell = \tau$. Indeed, the investigation of $B \rightarrow \gamma \tau^+ \tau^-$ decay in model I and II types of the 2HDM in [8], and in MSSM in [7], including NHB effects report that the contribution from exchanging neutral Higgs bosons may be quite sizable for large values of $\tan \beta$, which is already favored by LEP experiments [11].

We investigated the $B \rightarrow \gamma \ell^+ \ell^-$ decay for $\ell = \tau$ in the model III type of the 2HDM in a previous paper [10]. In this work we extend this study with an emphasis on possible CP violation effects. The CP asymmetry is of great interest in high energy physics especially since its origin is still unclear. In the SM, the source of CP violation is the complex CKM matrix elements, which can explain all the existing data on CP violation. However, for example, to explain the matter-antimatter asymmetry observed in the universe today one needs additional sources of CP violating effects, which has motivated to search new models beyond the SM. In model III type of the 2HDM, the complex Yukawa couplings provide a possible source of CP violation. Indeed, it was reported [12]-[14] that a measurable CP asymmetry was obtained due to this new phase in the model III.

The paper is organized as follows: In section 2, we first present the leading order (LO) QCD corrected effective Hamiltonian for the quark level process $b \rightarrow \gamma \ell^+ \ell^-$, including the NHB exchanges. Then we give the corresponding matrix element for the exclusive $B \rightarrow \gamma \ell^+ \ell^-$ decay. Next, we calculate the the forward-backward asymmetry of the lepton pair, A_{FB} , CP-violating asymmetry, A_{CP} , and the CP-violating asymmetry in forward-backward asymmetry,

$A_{CP}(A_{FB})$, as functions of the model parameters. Section 3 is devoted to the numerical analysis of these physical quantities with respect to the CP parameter $\sin \theta$, Yukawa couplings $\bar{\xi}_{N,\tau\tau}^D$ and $\bar{\xi}_{N,bb}^D$ and the mass ratio m_{h^0}/m_{A^0} and to the discussion of our results. In Appendix A, we give a brief summary about the general 2HDM (model III). The operators and the corresponding Wilson coefficients appearing in the effective Hamiltonian are given in Appendices B and C, respectively. Finally, some parametrizations used in the text may be found in Appendix D.

2. The exclusive $B \rightarrow \gamma \ell^+ \ell^-$ decay

The exclusive $B \rightarrow \gamma \ell^+ \ell^-$ decay is induced by the inclusive $b \rightarrow s \gamma \ell^+ \ell^-$ one. Therefore, we start with the QCD corrected effective Hamiltonian for the related quark level process $b \rightarrow s \ell^+ \ell^-$, which is obtained by integrating out heavy particles in the SM and in the 2HDM [15, 16]

$$\mathcal{H} = \frac{-4G_F}{\sqrt{2}} V_{tb} V_{ts}^* \left\{ \sum_{i=1}^{10} C_i(\mu) O_i(\mu) + \sum_{i=1}^{10} C_{Q_i}(\mu) Q_i(\mu) \right\}, \quad (1)$$

where O_i are current-current ($i = 1, 2$), penguin ($i = 1, \dots, 6$), magnetic penguin ($i = 7, 8$) and semileptonic ($i = 9, 10$) operators. The additional operators Q_i , ($i = 1, \dots, 10$) are due to the NHB exchange diagrams, which give considerable contributions in the case that the lepton pair is $\tau^+ \tau^-$ [15]. $C_i(\mu)$ and $C_{Q_i}(\mu)$ are Wilson coefficients renormalized at the scale μ . All these operators and the Wilson coefficients, together with their initial values calculated at $\mu = m_W$ in the SM and also the additional coefficients coming from the new Higgs scalars are presented in Appendices B and C.

Neglecting the strange quark mass, the effective Hamiltonian (1) leads to the following matrix element for $b \rightarrow s \ell^+ \ell^-$,

$$\begin{aligned} \mathcal{M} = & \frac{\alpha G_F}{\sqrt{2} \pi} V_{tb} V_{ts}^* \left\{ C_9^{eff} (\bar{s} \gamma_\mu P_L b) \bar{\ell} \gamma_\mu \ell + C_{10} (\bar{s} \gamma_\mu P_L b) \bar{\ell} \gamma_\mu \gamma_5 \ell \right. \\ & \left. - 2C_7 \frac{m_b}{q^2} (\bar{s} i \sigma_{\mu\nu} q_\nu P_R b) \bar{\ell} \gamma_\mu \ell + C_{Q_1} (\bar{s} P_R b) \bar{\ell} \ell + C_{Q_2} (\bar{s} P_R b) \bar{\ell} \gamma_5 \ell \right\}, \quad (2) \end{aligned}$$

where $P_{L,R} = (1 \mp \gamma_5)/2$, q is the momentum transfer and V_{ij} 's are the corresponding elements of the CKM matrix.

In order to obtain the matrix element for $b \rightarrow s \gamma \ell^+ \ell^-$ decay, a photon line should be attached to any charged internal or external line. As pointed out before [5, 6], contributions coming from the release of the free photon from any charged internal line will be suppressed by a factor of m_b^2/M_W^2 and we neglect them in the following analysis. When a photon is released from the initial quark lines

it contributes to the so-called "structure dependent" (SD) part of the amplitude. Using the expressions

$$\begin{aligned} \langle \gamma(k) | \bar{s} \gamma_\mu (1 \mp \gamma_5) b | B(p_B) \rangle &= \frac{e}{m_B^2} \left\{ \epsilon_{\mu\nu\lambda\sigma} \varepsilon^{*\nu} q^\lambda k^\sigma g(q^2) \pm i \left[\varepsilon^{*\mu}(kq) - (\varepsilon^* q) k^\mu \right] f(q^2) \right\}, \\ \langle \gamma | \bar{s} i \sigma_{\mu\nu} k_\nu (1 \mp \gamma_5) b | B \rangle &= \frac{e}{m_B^2} \left\{ \epsilon_{\mu\alpha\beta\sigma} \epsilon_\alpha^* k_\beta q_\sigma g_1(p^2) \mp i \left[\epsilon_\mu^*(kq) - (\epsilon^* k) q_\mu \right] f_1(p^2) \right\}, \\ \langle \gamma | \bar{s} (1 + \gamma_5) b | B \rangle &= 0, \end{aligned} \quad (3)$$

the SD part of the amplitude can be written as

$$\begin{aligned} \mathcal{M}_{SD} &= \frac{\alpha G_F}{2\sqrt{2}\pi} V_{tb} V_{ts}^* \frac{e}{m_B^2} \left\{ \bar{\ell} \gamma^\mu \ell \left[A_1 \epsilon_{\mu\nu\alpha\beta} \varepsilon^{*\nu} q^\alpha k^\beta + i A_2 \left(\varepsilon_\mu^*(kq) - (\varepsilon^* q) k_\mu \right) \right] \right. \\ &\quad \left. + \bar{\ell} \gamma^\mu \gamma_5 \ell \left[B_1 \epsilon_{\mu\nu\alpha\beta} \varepsilon^{*\nu} q^\alpha k^\beta + i B_2 \left(\varepsilon_\mu^*(kq) - (\varepsilon^* q) k_\mu \right) \right] \right\}, \end{aligned} \quad (4)$$

where ε_μ^* and k_μ are the four vector polarization and four momentum of the photon, respectively, and p_B is the momentum of the B meson. In Eq. (4), A_1 , A_2 , B_1 and B_2 are functions of the Wilson coefficients and the form factors, and they are given in Appendix D.

We note that the neutral Higgs exchange interactions do not contribute to the structure dependent part of the matrix element \mathcal{M}_{SD} . However, the situation is different for the so-called "internal Bremsstrahlung" (IB) contribution, \mathcal{M}_{IB} , which arises when a photon is radiated from one of the final ℓ -leptons. Using the expressions

$$\begin{aligned} \langle 0 | \bar{s} \gamma_\mu \gamma_5 b | B \rangle &= -i f_B P_{B\mu}, \\ \langle 0 | \bar{s} \sigma_{\mu\nu} (1 \pm \gamma_5) b | B \rangle &= 0, \\ \langle 0 | \bar{s} \gamma_5 b | B \rangle &= i f_B \frac{m_B^2}{m_b}, \\ \langle 0 | \bar{s} b | B \rangle &= 0, \end{aligned} \quad (5)$$

and the conservation of the vector current, IB part of the matrix element is found as [8]

$$\begin{aligned} \mathcal{M}_{IB} &= \frac{\alpha G_F}{2\sqrt{2}\pi} V_{tb} V_{ts}^* e f_B i \left\{ F \bar{\ell} \left(\frac{\not{\epsilon}^* \not{p}_B}{2p_1 k} - \frac{\not{p}_B \not{\epsilon}^*}{2p_2 k} \right) \gamma_5 \ell \right. \\ &\quad \left. + F_1 \bar{\ell} \left[\frac{\not{\epsilon}^* \not{p}_B}{2p_1 k} - \frac{\not{p}_B \not{\epsilon}^*}{2p_2 k} + 2m_\ell \left(\frac{1}{2p_1 k} + \frac{1}{2p_2 k} \right) \not{\epsilon}^* \right] \ell \right\}, \end{aligned} \quad (6)$$

where F and F_1 are functions of form factors and the Wilson coefficients C_{Q_1} and C_{Q_2} due to the NHB effects and their explicit forms can be found in Appendix D. Finally, the total matrix element for the $B \rightarrow \gamma \ell^+ \ell^-$ decay is obtained as a sum of the \mathcal{M}_{SD} and \mathcal{M}_{IB} terms, $\mathcal{M} = \mathcal{M}_{SD} + \mathcal{M}_{IB}$.

Now, we will calculate the forward-backward asymmetry, A_{FB} , for the lepton pair, CP-violating asymmetry, A_{CP} , and CP violating asymmetry in the forward-backward asymmetry, $A_{CP}(A_{FB})$ for the process under consideration. All these measurable physical quantities can provide a great deal of clues to test the theoretical models used. We first give the definitions of $A_{FB}(x)$ and A_{CP} :

$$A_{FB}(x) = \frac{\int_0^1 dz \frac{d^2\Gamma}{dxdz} - \int_{-1}^0 dz \frac{d^2\Gamma}{dxdz}}{\int_0^1 dz \frac{d^2\Gamma}{dxdz} + \int_{-1}^0 dz \frac{d^2\Gamma}{dxdz}}, \quad (7)$$

$$A_{CP} = \frac{\Gamma(B \rightarrow \gamma \ell^+ \ell^-) - \Gamma(\bar{B} \rightarrow \gamma \ell^+ \ell^-)}{\Gamma(B \rightarrow \gamma \ell^+ \ell^-) + \Gamma(\bar{B} \rightarrow \gamma \ell^+ \ell^-)}, \quad (8)$$

where $z = \cos \theta$, θ is the angle between the momentum of the B-meson and that of ℓ^- and $x = 2E_\gamma/m_B$ is the dimensionless photon energy. In Eq.(7), $\frac{d^2\Gamma}{dxdz}$ is the double differential decay rate and in the center of mass (CM) frame of the dileptons $\ell^+ \ell^-$, it is given by

$$\begin{aligned} \frac{d^2\Gamma}{dxdz} = & \left| \frac{\alpha G_F}{2\sqrt{2}\pi} V_{tb} V_{ts}^* \right|^2 \frac{\alpha}{(2\pi)^3} \frac{\pi}{4} m_B x v \\ & \left\{ \frac{m_B^2}{32} x^2 \left[((1+z^2)(1-x-4r))(|A_1|^2 + |A_2|^2 + |B_1|^2 + |B_2|^2) \right. \right. \\ & + 8r(|A_1|^2 + |A_2|^2) + 4z\sqrt{(1-x)(1-x-4r)} \text{Re}(A_2 B_1^* + A_1 B_2^*) \left. \right] \\ & + f_B m_\ell \frac{(x-1)}{((z^2-1)(x-1) + 4rz^2)} \left[vxz \text{Re}(B_2 F^* - B_1 F_1^*) \right. \\ & + (1-4r-z^2(1-x-4r)) \text{Re}(A_2 F_1^*) - x \text{Re}(A_1 F^*) \left. \right] \\ & + f_B^2 \frac{(1-x)}{x^2((z^2-1)(x-1) + 4rz^2)^2} \left[|F|^2 ((-2+4x-3x^2+x^3) \right. \\ & + 8r(1-x)(z^2-1) + 4rx^2z^2) + |F_1|^2 ((32r^2(x-1) + 4r(4-6x+2x^2) \right. \\ & \left. \left. - 2+4x-3x^2+x^3)(z^2-1) + x^2z^2 \right) \right] \right\}. \end{aligned} \quad (9)$$

where $v = \sqrt{1 - \frac{4r}{1-x}}$ with $r = m_\ell^2/m_B^2$. Integrating over the angle variable, we

find the forward backward asymmetry A_{FB} as follows,

$$A_{FB} = - \int dx 4v x^2 \left\{ m_B^2 x \sqrt{(x-1)(x-1+4r)} \operatorname{Re}(A_1 A_2^* - B_1 B_2^*) \right. \\ \left. - 4f_B m_\ell v \left(\frac{x-1}{x-1+4r} \right) \ln \frac{4r}{1-x} \operatorname{Re}((A_2 - B_2) F^* \right. \\ \left. - (A_1 - B_1) F_1^*) \right\} \left/ \int dx D(x) \right., \quad (10)$$

where

$$D(x) = \frac{m_B^2}{12} x^3 v \left[(|A_1|^2 + |A_2|^2)(1+2r-x) + (|B_1|^2 + |B_2|^2)(1-4r-x) \right] \\ - f_B m_\ell x \left[2v(1-x) \operatorname{Re}(A_2 F_1^*) + \ln \frac{1+v}{1-v} \left((x-4r) \operatorname{Re}(A_2 F_1^*) - x \operatorname{Re}(A_1 F^*) \right) \right] \\ - 2f_B^2 \left[v \frac{(1-x)}{x} \left(|F|^2 + (1-4r) |F_1|^2 \right) + \ln \frac{1+v}{1-v} \left(\left(1 + \frac{2r}{x} - \frac{1}{x} - \frac{x}{2} \right) |F|^2 \right. \right. \\ \left. \left. + \left((1-4r) - \frac{2(1-6r+8r^2)}{x} - \frac{x}{2} \right) |F_1|^2 \right) \right]. \quad (11)$$

We note that in these integrals the Dalitz boundary for the dimensionless photon energy x is taken as

$$\delta \leq x \leq 1 - \frac{4m_\ell^2}{m_B^2}, \quad (12)$$

since $|\mathcal{M}_{IB}|^2$ term has infrared singularity due to the emission of soft photon. In order to obtain a finite result, we follow the approach described in ref.[6] and impose a cut on the photon energy, i.e., we require $E_\gamma \geq 50$ MeV, which corresponds to detecting only hard photons experimentally. This cut requires that $E_\gamma \geq \delta m_B/2$ with $\delta = 0.01$.

For $B \rightarrow \gamma \ell^+ \ell^-$ decay, A_{CP} almost vanishes in the SM due to the unitarity of CKM matrix together with the smallness of $V_{ub} V_{us}^*$. However, in model III complex Yukawa couplings provide a new source of CP violation. In our calculations, we choose $\bar{\xi}_{N,bb}^D = |\bar{\xi}_{N,bb}^D| e^{i\theta}$ so that C_9^{eff} , C_{Q_1} and C_{Q_2} are the Wilson coefficients that contain CP violating terms. Using Eq.(8), we calculate A_{CP} as

$$A_{CP} = \frac{\int dx T(x)}{\int dx (D(x) + D_{CP}(x))}, \quad (13)$$

where

$$T(x) = m_B^2 x^2 \operatorname{Im}(\bar{\xi}_{N,bb}^D) \left\{ \frac{v}{3} x (1 + 2r - x) A_1^{(2)} A_1^{(3)} - 2f_B \frac{m_\ell}{m_b} \left[\left(2v(1 - x) + (x - 4r) \ln \frac{1 + v}{1 - v} \right) A_2^{(2)} F_1^{(2)} - x \ln \frac{1 + v}{1 - v} A_1^{(2)} F^{(2)} \right] \right\}, \quad (14)$$

and $D_{CP}(x)$ is the CP conjugate of $D(x)$ which is defined as

$$D_{CP}(x) = D(x) \left(\bar{\xi}_{N,bb}^D \rightarrow (\bar{\xi}_{N,bb}^D)^* \right). \quad (15)$$

The explicit form of the functions $A_{(1)}^{(2)}$, $A_{(1)}^{(3)}$, etc., in Eq.(14) are given in Appendix D.

Finally, we consider the CP violating asymmetry in A_{FB} , $A_{CP}(A_{FB})$, which is an important measurable quantity that may provide information about the model used. It is defined as

$$A_{CP}(A_{FB}) = \frac{A_{FB} - \bar{A}_{FB}}{A_{FB} + \bar{A}_{FB}}, \quad (16)$$

Here, A_{FB} is given by Eq.(10) and \bar{A}_{FB} is obtained by the replacement $\bar{\xi}_{N,bb}^D \rightarrow (\bar{\xi}_{N,bb}^D)^*$ in A_{FB} .

3. Numerical analysis and discussion

We present here our numerical results only for $\ell = \tau$ channel, but they can easily be applied to the $\ell = \mu$ case. The input parameters we used in our numerical analysis are as follows:

$$\begin{aligned} m_B &= 5.28 \text{ GeV}, \quad m_b = 4.8 \text{ GeV}, \quad m_c = 1.4 \text{ GeV}, \quad m_\tau = 1.78 \text{ GeV}, \\ m_{H^0} &= 150 \text{ GeV}, \quad m_{h^0} = 70 \text{ GeV}, \quad m_{A^0} = 80 \text{ GeV}, \quad m_{H^\pm} = 400 \text{ GeV}, \\ |V_{tb} V_{ts}^*| &= 0.045, \quad \alpha^{-1} = 129, \quad G_F = 1.17 \times 10^{-5} \text{ GeV}^{-2}, \quad \tau_B = 1.64 \times 10^{-12} \text{ s}, \\ C_9^{eff} &= 4.229, \quad C_{10} = -4.659. \end{aligned} \quad (17)$$

Here we note that the value of the Wilson coefficient C_9^{eff} above corresponds to only the short-distance contributions. C_9^{eff} also receives long-distance (LD) contributions associated with the real $\bar{c}c$ intermediate states (See Appendix C for the details of LD contributions). There are five possible resonances in the $\bar{c}c$ system that can contribute to the $B \rightarrow \gamma \tau^+ \tau^-$ decay and to calculate their contributions we need to divide the integration region for x into two parts: $\delta \leq x \leq 1 - ((m_{\psi_2} +$

$0.02)/m_B)^2$ and $1 - ((m_{\psi_2} - 0.02)/m_B)^2 \leq x \leq 1 - (2m_\tau/m_B)^2$, where $m_{\psi_2} = 3.686$ GeV is the mass of the second resonance.

For the values of the form factors g , f , g_1 and f_1 , we have used the results of ref. [17] and [18], and represent their q^2 dependencies in terms of two parameters $F(0)$ and m_F as

$$F(q^2) = \frac{F(0)}{\left(1 - \frac{q^2}{m_F^2}\right)^2} \quad (18)$$

where the values $F(0)$ and m_F for the $B \rightarrow \gamma$ are listed in Table 1.

There are many free parameters in the general 2HDM, such as masses of the charged and neutral Higgs bosons and complex Yukawa couplings, $\xi_{ij}^{U,D}$, where i, j are quark flavor indices. There are also some experimental results that one can use to restrict these new parameters. In this context, the stronger restriction comes from the analysis of the $\Delta F = 2$ decays with $F = K, B_d, D$ mesons, the ρ parameter and the $B \rightarrow X_s \gamma$ decay.

The contributions to the Wilson coefficient C_7 from the neutral Higgs bosons h^0 and A^0 are given by [19]

$$C_7^H(m_W) = (V_{tb}V_{ts}^*)^{-1} \sum_{i=d,s,b} \bar{\xi}_{N,bi}^D \bar{\xi}_{N,is}^D \frac{Q_i}{8m_i m_b}, \quad (19)$$

where $H = h^0, A^0$, and m_i and Q_i are the masses and charges of the down quarks, respectively. Eq. (19) shows that the neutral Higgs bosons can give a large contribution to the Wilson coefficient C_7 and this contradicts with the CLEO data [3]

$$BR(B \rightarrow X_s \gamma) = (3.15 \pm 0.35 \pm 0.32) \times 10^{-4}. \quad (20)$$

However, assuming that the couplings $\bar{\xi}_{N,is}^D$ with $i = d, s, b$ and $\bar{\xi}_{N,bd}^D$ are small enough to reach the conditions $\bar{\xi}_{N,bb}^D \bar{\xi}_{N,is}^D \ll 1$ and $\bar{\xi}_{N,bd}^D \bar{\xi}_{N,ds}^D \ll 1$ [19], together with the constraints from $\Delta F = 2$ mixing [20] and the ρ parameter [21], we obtain the conditions

$$\begin{aligned} \bar{\xi}_{N,tc} &\ll \bar{\xi}_{N,tt}^U, \\ \bar{\xi}_{N,ib}^D &\quad , \quad \bar{\xi}_{N,ij}^D \sim 0 \quad i, j = d, s, \end{aligned} \quad (21)$$

so that we only take into account $\bar{\xi}_{N,tt}^U$ and $\bar{\xi}_{N,bb}^D$. In our work, we choose $\bar{\xi}_{N,tt}^U$ as real and $\bar{\xi}_{N,bb}^D$ as complex, namely $\bar{\xi}_{N,bb}^D = |\bar{\xi}_{N,bb}^D|e^{i\theta}$. As for the $\bar{\xi}_{N,\tau\tau}^U$, since it controls the contributions due to the NHB effects, we leave $\bar{\xi}_{N,\tau\tau}^U$ as a free parameter to investigate the size of NHB effect on the measurable quantities of the $B \rightarrow \gamma \tau^+ \tau^-$ decay.

In our numerical calculations, we further adopted the constraint on the Wilson coefficient C_7^{eff} , $0.257 \leq |C_7^{eff}| \leq 0.439$ [20] due to the CLEO measurement (Eq.(20)) and the redefinition

$$\xi^{U,D} = \sqrt{\frac{4G_F}{\sqrt{2}}} \bar{\xi}^{U,D} .$$

The above constraint on the C_7^{eff} restricts the allowed regions of the measurable quantities of the exclusive $B \rightarrow \gamma \tau^+ \tau^-$ decay, namely, A_{FB} , A_{CP} and $A_{CP}(A_{FB})$ and these regions are represented by the ones between the solid curves for $C_7^{eff} > 0$ and the dashed curves for $C_7^{eff} < 0$ throughout the graphs in Figs. 1-18.

In Fig. 1, we plot $\sin \theta$ dependence of A_{FB} without NHB effects for the case of ratio $|r_{tb}| \equiv \left| \frac{\xi_{N,tt}^U}{\xi_{N,bb}^D} \right| < 1$. We see that in model III without NHB effects, $|A_{FB}|$ is smaller compared to its value in the SM (0.183), represented by the dashed straight line, for $C_7^{eff} > 0$, but it can be enhanced up to 7% with increasing $\sin \theta$. For $C_7^{eff} < 0$, A_{FB} is not much sensitive to $\sin \theta$, but its value can be slightly greater than the SM prediction. Including the NHB effects to A_{FB} (Fig. 2) reduces its magnitude 30% of its value without NHB effects for $C_7^{eff} > 0$, while for $C_7^{eff} < 0$, A_{FB} is almost the same as the SM value.

In Fig. 3 (4), we present A_{FB} as a function of $\bar{\xi}_{N,bb}^D (m_{h^0}/m_{A^0})$ for $\bar{\xi}_{N,\tau\tau}^D = 10 m_\tau$, $\sin \theta = 0.5$ and $|r_{tb}| < 1$. A_{FB} is at the order of magnitude 10^{-1} and increases with the increasing values of both $\bar{\xi}_{N,bb}^D$ and m_{h^0}/m_{A^0} . For $C_7^{eff} > 0$, A_{FB} stands less than the SM prediction and for $C_7^{eff} < 0$, model III prediction can reach the SM one for large values of $\bar{\xi}_{N,bb}^D$ and m_{h^0}/m_{A^0} .

We have also calculated the $\sin \theta$ ($\bar{\xi}_{N,bb}^D$ and m_{h^0}/m_{A^0}) dependence of A_{FB} for the case of ratio $r_{tb} > 1$. We have found that in this case A_{FB} is one (two) order(s) of magnitude smaller than its value for $|r_{tb}| < 1$ case, and including NHB effects reduces this value even one more order of magnitude. Therefore we do not present these graphs here.

Fig. 5 represents $\sin \theta$ dependence of A_{CP} without NHB effects for the case of ratio $|r_{tb}| < 1$. It is at the order of magnitude 10^{-2} and increases with $\sin \theta$. For $C_7^{eff} < 0$, A_{CP} can have both signs, while for $C_7^{eff} > 0$ its sign does not change in the restricted region. Including the NHB effects (Fig. 6) reduces $|A_{CP}|$ without NHB effects almost by 60% for $C_7^{eff} > 0$. However, for $C_7^{eff} < 0$, it is possible to enhance it by up to 35%.

Figs. 8 and 7 are devoted to $\sin \theta$ dependence of A_{CP} for $r_{tb} > 1$ with and without NHB effects, respectively. Without NHB effects, $|A_{CP}|$ is at the order of magnitude 10^{-3} and including the NHB effects can enhance it up to two orders

of magnitude, i.e., it becomes $|A_{CP}| \sim 10^{-1}$. We further note that the restricted region for $C_7^{eff} > 0$ (solid lines) and $C_7^{eff} < 0$ (dashed lines) are now larger but they almost coincide.

Fig. 9 (10) shows A_{CP} as a function of $\bar{\xi}_{N,\tau\tau}^D$ for $\bar{\xi}_{N,bb}^D = 40(0.1)m_b$ and $\sin\theta = 0.5$ for $|r_{tb}| < 1$ ($r_{tb} > 1$). We see that A_{CP} is sensitive to the parameter $\bar{\xi}_{N,\tau\tau}^D$ and it decreases (increases) with the increasing values of $\bar{\xi}_{N,\tau\tau}^D$ for $C_7^{eff} > 0$ ($C_7^{eff} < 0$) when $|r_{tb}| < 1$. When $r_{tb} > 1$, restricted regions for $C_7^{eff} > 0$ (solid lines) and $C_7^{eff} < 0$ (dashed lines) almost coincide and $|A_{CP}|$ can take one orders of magnitude larger values compared to the case where $|r_{tb}| < 1$.

In Fig. 11 (12), we plot the dependence of A_{CP} on m_{h^0}/m_{A^0} for $\bar{\xi}_{N,\tau\tau}^D = 10(1)m_\tau$, $\bar{\xi}_{N,bb}^D = 40(0.1)m_b$ and $\sin\theta = 0.5$ for $|r_{tb}| < 1$ ($r_{tb} > 1$). For $|r_{tb}| < 1$ and $C_7^{eff} > 0$, A_{CP} is sensitive to the ratio m_{h^0}/m_{A^0} and increases with the increasing values of m_{h^0}/m_{A^0} . However, for $C_7^{eff} < 0$, dependence of A_{CP} on the ratio is weak but, the restricted region is larger this time. As seen from Fig. 12, when $r_{tb} > 1$, $|A_{CP}|$ can take one orders of magnitude larger values compared to the case where $|r_{tb}| < 1$.

Finally, we present our results about the CP violating asymmetry in A_{FB} , $A_{CP}(A_{FB})$ in a series of figures, Figs.13-18. Fig. 13 (14) shows $A_{CP}(A_{FB})$ as a function of $\sin\theta$ for $\bar{\xi}_{N,\tau\tau}^D = 10(1)m_\tau$, $\bar{\xi}_{N,bb}^D = 40(0.1)m_b$ for $|r_{tb}| < 1$ ($r_{tb} > 1$). For $|r_{tb}| < 1$, $A_{CP}(A_{FB})$ is at the order of magnitude 10^{-2} and it does not change sign in the restricted region for $C_7^{eff} > 0$, while it can have both signs for $C_7^{eff} < 0$. For $r_{tb} > 1$, $A_{CP}(A_{FB})$ can reach 5% for the intermediate values of $\sin\theta$ and restricted regions for $C_7^{eff} > 0$ (solid lines) and $C_7^{eff} < 0$ (dashed lines) almost coincide.

We can see from Figs.15 and 16 that $A_{CP}(A_{FB})$ is sensitive to the parameter $\bar{\xi}_{N,\tau\tau}^D$, especially for its small values. $A_{CP}(A_{FB})$ is a decreasing (increasing) function of $\bar{\xi}_{N,\tau\tau}^D$ for $|r_{tb}| < 1$ ($r_{tb} > 1$) and reaches 1(6)% for $\bar{\xi}_{N,\tau\tau}^D = 1(50)$.

Fig. 17 (18) is devoted to the ratio m_{h^0}/m_{A^0} dependence of $A_{CP}(A_{FB})$ for $\bar{\xi}_{N,\tau\tau}^D = 10(1)m_\tau$, $\bar{\xi}_{N,bb}^D = 40(0.1)m_b$ and $\sin\theta = 0.5$ for $|r_{tb}| < 1$ ($r_{tb} > 1$). It is seen from Fig. 17 that for $|r_{tb}| < 1$, $A_{CP}(A_{FB})$ is sensitive to the mass ratio m_{h^0}/m_{A^0} and it is increasing with the increasing values of m_{h^0}/m_{A^0} for $C_7^{eff} > 0$, while for $C_7^{eff} < 0$, its dependence on the mass ratio is weak. For $r_{tb} > 1$, $|A_{CP}(A_{FB})|$ is one order of magnitude larger than its value for $|r_{tb}| < 1$.

In conclusion, we have investigated the physical quantities A_{FB} , A_{CP} and $A_{CP}(A_{FB})$ for the exclusive $B \rightarrow \gamma \ell^+ \ell^-$ decay in the general 2HDM including the NHB effects. From the results we have obtained we conclude that experimental investigation of these quantities may be very useful for testing the new physics effects beyond the SM and also the sign of C_7^{eff} .

	$F(0)$	a_F
g	1 GeV	5.6 GeV
f	0.8 GeV	6.5 GeV
g_1	3.74 GeV^2	6.4 GeV
f_1	0.68 GeV^2	5.5 GeV

Table 1. B meson decay form factors in the light-cone QCD sum rule.

Appendix A

Model Description

The 2HDM is the minimal extension of the SM, which consists of adding a second doublet to the Higgs sector. In this model, there are one charged Higgs scalar, two neutral Higgs scalars and one neutral Higgs pseudoscalar. The general Yukawa Lagrangian, which is responsible for the interactions of quarks with gauge bosons, can be written as

$$\mathcal{L}_Y = \eta_{ij}^U \bar{Q}_{iL} \tilde{\phi}_1 U_{jR} + \eta_{ij}^D \bar{Q}_{iL} \phi_1 D_{jR} + \xi_{ij}^{U\dagger} \bar{Q}_{iL} \tilde{\phi}_2 U_{jR} + \xi_{ij}^D \bar{Q}_{iL} \phi_2 D_{jR} + \text{h.c.} \quad (\text{A.1})$$

where i, j are family indices of quarks, L and R denote chiral projections $L(R) = 1/2(1 \mp \gamma_5)$, ϕ_m for $m = 1, 2$, are the two scalar doublets, Q_{iL} are quark doublets, U_{jR} , D_{jR} are the corresponding quark singlets, $\eta_{ij}^{U,D}$ and $\xi_{ij}^{U,D}$ are the matrices of the Yukawa couplings. The Yukawa Lagrangian in Eq. (A.1) opens up the possibility that there appear tree-level FCNC, which are forbidden in the SM and model I and model II types of the 2HDM. However, tree-level FCNC are permitted in the general 2HDM, and this type of 2HDM is referred to as model III in the literature.

In this model, it is possible to choose ϕ_1 and ϕ_2 in the following form

$$\phi_1 = \frac{1}{\sqrt{2}} \left[\begin{pmatrix} 0 \\ v + H^0 \end{pmatrix} + \begin{pmatrix} \sqrt{2}\chi^+ \\ i\chi^0 \end{pmatrix} \right]; \phi_2 = \frac{1}{\sqrt{2}} \begin{pmatrix} \sqrt{2}H^+ \\ H_1 + iH_2 \end{pmatrix}, \quad (\text{A.2})$$

with the vacuum expectation values,

$$\langle \phi_1 \rangle = \frac{1}{\sqrt{2}} \begin{pmatrix} 0 \\ v \end{pmatrix}; \langle \phi_2 \rangle = 0. \quad (\text{A.3})$$

With this choice, the SM particles can be collected in the first doublet and the new particles in the second one. Further, we take H_1, H_2 as the mass eigenstates h^0 ,

A^0 respectively. Note that, at tree level, there is no mixing among CP even neutral Higgs bosons, namely the SM one, H^0 , and beyond, h^0 .

The part which produces FCNC at tree level is

$$\mathcal{L}_{Y,FC} = \xi_{ij}^{U\dagger} \bar{Q}_{iL} \tilde{\phi}_2 U_{jR} + \xi_{ij}^D \bar{Q}_{iL} \phi_2 D_{jR} + \xi_{kl}^D \bar{l}_k L \phi_2 E_{lR} + h.c. . \quad (\text{A.4})$$

In Eq.(A.4), the couplings $\xi^{U,D}$ for the flavor-changing charged interactions are

$$\begin{aligned} \xi_{ch}^U &= \xi_{neutral} V_{CKM} , \\ \xi_{ch}^D &= V_{CKM} \xi_{neutral} , \end{aligned} \quad (\text{A.5})$$

where $\xi_{neutral}^{U,D}$ is defined by the expression

$$\xi_N^{U(D)} = (V_{R(L)}^{U(D)})^{-1} \xi^{U,(D)} V_{L(R)}^{U(D)} , \quad (\text{A.6})$$

and $\xi_{neutral}^{U,D}$ is denoted as $\xi_N^{U,D}$. Here the charged couplings are the linear combinations of neutral couplings multiplied by V_{CKM} matrix elements (see [20] for details).

Appendix B

The operator basis

The operator basis in the general 2HDM (model III) for our process is [15, 16, 22, 23]

$$\begin{aligned} O_1 &= (\bar{s}_{L\alpha} \gamma_\mu c_{L\beta})(\bar{c}_{L\beta} \gamma^\mu b_{L\alpha}) , \quad O_2 = (\bar{s}_{L\alpha} \gamma_\mu c_{L\alpha})(\bar{c}_{L\beta} \gamma^\mu b_{L\beta}) , \\ O_3 &= (\bar{s}_{L\alpha} \gamma_\mu b_{L\alpha}) \sum_{q=u,d,s,c,b} (\bar{q}_{L\beta} \gamma^\mu q_{L\beta}) , \quad O_4 = (\bar{s}_{L\alpha} \gamma_\mu b_{L\beta}) \sum_{q=u,d,s,c,b} (\bar{q}_{L\beta} \gamma^\mu q_{L\alpha}) , \\ O_5 &= (\bar{s}_{L\alpha} \gamma_\mu b_{L\alpha}) \sum_{q=u,d,s,c,b} (\bar{q}_{R\beta} \gamma^\mu q_{R\beta}) , \quad O_6 = (\bar{s}_{L\alpha} \gamma_\mu b_{L\beta}) \sum_{q=u,d,s,c,b} (\bar{q}_{R\beta} \gamma^\mu q_{R\alpha}) , \\ O_7 &= \frac{e}{16\pi^2} \bar{s}_\alpha \sigma_{\mu\nu} (m_b R + m_s L) b_\alpha \mathcal{F}^{\mu\nu} , \quad O_8 = \frac{g}{16\pi^2} \bar{s}_\alpha T_{\alpha\beta}^a \sigma_{\mu\nu} (m_b R + m_s L) b_\beta \mathcal{G}^{a\mu\nu} , \\ O_9 &= \frac{e}{16\pi^2} (\bar{s}_{L\alpha} \gamma_\mu b_{L\alpha})(\bar{\ell} \gamma^\mu \ell) , \quad O_{10} = \frac{e}{16\pi^2} (\bar{s}_{L\alpha} \gamma_\mu b_{L\alpha})(\bar{\ell} \gamma^\mu \gamma_5 \ell) , \\ Q_1 &= \frac{e^2}{16\pi^2} (\bar{s}_L^\alpha b_R^\alpha)(\bar{\ell} \ell) , \quad Q_2 = \frac{e^2}{16\pi^2} (\bar{s}_L^\alpha b_R^\alpha)(\bar{\ell} \gamma_5 \ell) , \\ Q_3 &= \frac{g^2}{16\pi^2} (\bar{s}_L^\alpha b_R^\alpha) \sum_{q=u,d,s,c,b} (\bar{q}_L^\beta q_R^\beta) , \quad Q_4 = \frac{g^2}{16\pi^2} (\bar{s}_L^\alpha b_R^\alpha) \sum_{q=u,d,s,c,b} (\bar{q}_R^\beta q_L^\beta) , \\ Q_5 &= \frac{g^2}{16\pi^2} (\bar{s}_L^\alpha b_R^\beta) \sum_{q=u,d,s,c,b} (\bar{q}_L^\beta q_R^\alpha) , \quad Q_6 = \frac{g^2}{16\pi^2} (\bar{s}_L^\alpha b_R^\beta) \sum_{q=u,d,s,c,b} (\bar{q}_R^\beta q_L^\alpha) , \end{aligned} \quad (\text{B.1})$$

$$\begin{aligned}
Q_7 &= \frac{g^2}{16\pi^2} (\bar{s}_L^\alpha \sigma^{\mu\nu} b_R^\alpha) \sum_{q=u,d,s,c,b} (\bar{q}_L^\beta \sigma_{\mu\nu} q_R^\beta), \quad Q_8 = \frac{g^2}{16\pi^2} (\bar{s}_L^\alpha \sigma^{\mu\nu} b_R^\alpha) \sum_{q=u,d,s,c,b} (\bar{q}_R^\beta \sigma_{\mu\nu} q_L^\beta), \\
Q_9 &= \frac{g^2}{16\pi^2} (\bar{s}_L^\alpha \sigma^{\mu\nu} b_R^\beta) \sum_{q=u,d,s,c,b} (\bar{q}_L^\beta \sigma_{\mu\nu} q_R^\alpha), \quad Q_{10} = \frac{g^2}{16\pi^2} (\bar{s}_L^\alpha \sigma^{\mu\nu} b_R^\beta) \sum_{q=u,d,s,c,b} (\bar{q}_R^\beta \sigma_{\mu\nu} q_L^\alpha)
\end{aligned}$$

where α and β are $SU(3)$ colour indices and $\mathcal{F}^{\mu\nu}$ and $\mathcal{G}^{\mu\nu}$ are the field strength tensors of the electromagnetic and strong interactions, respectively. Note that there are also flipped chirality partners of these operators, which can be obtained by interchanging L and R in the basis given above in model III. However, we do not present them here since corresponding Wilson coefficients are negligible.

Appendix C

The Initial values of the Wilson coefficients.

The initial values of the Wilson coefficients for the relevant process in the SM are [22]

$$\begin{aligned}
C_{1,3,\dots,6}^{SM}(m_W) &= 0, \\
C_2^{SM}(m_W) &= 1, \\
C_7^{SM}(m_W) &= \frac{3x_t^3 - 2x_t^2}{4(x_t - 1)^4} \ln x_t + \frac{-8x_t^3 - 5x_t^2 + 7x_t}{24(x_t - 1)^3}, \\
C_8^{SM}(m_W) &= -\frac{3x_t^2}{4(x_t - 1)^4} \ln x_t + \frac{-x_t^3 + 5x_t^2 + 2x_t}{8(x_t - 1)^3}, \\
C_9^{SM}(m_W) &= -\frac{1}{\sin^2 \theta_W} B(x_t) + \frac{1 - 4 \sin^2 \theta_W}{\sin^2 \theta_W} C(x_t) - D(x_t) + \frac{4}{9}, \\
C_{10}^{SM}(m_W) &= \frac{1}{\sin^2 \theta_W} (B(x_t) - C(x_t)), \\
C_{Q_i}^{SM}(m_W) &= 0 \quad i = 1, \dots, 10
\end{aligned} \tag{C.1}$$

and for the additional part due to charged Higgs bosons are

$$\begin{aligned}
C_{1,\dots,6}^H(m_W) &= 0, \\
C_7^H(m_W) &= Y^2 F_1(y_t) + XY F_2(y_t), \\
C_8^H(m_W) &= Y^2 G_1(y_t) + XY G_2(y_t), \\
C_9^H(m_W) &= Y^2 H_1(y_t), \\
C_{10}^H(m_W) &= Y^2 L_1(y_t),
\end{aligned} \tag{C.2}$$

where

$$\begin{aligned} X &= \frac{1}{m_b} \left(\bar{\xi}_{N,bb}^D + \bar{\xi}_{N,sb}^D \frac{V_{ts}}{V_{tb}} \right) , \\ Y &= \frac{1}{m_t} \left(\bar{\xi}_{N,tt}^U + \bar{\xi}_{N,tc}^U \frac{V_{cs}^*}{V_{ts}^*} \right) . \end{aligned} \quad (\text{C.3})$$

The NHB effects bring new operators and the corresponding Wilson coefficients read as [24]

$$\begin{aligned} C_{Q_2}^{A^0}((\bar{\xi}_{N,tt}^U)^3) &= \frac{\bar{\xi}_{N,\tau\tau}^D (\bar{\xi}_{N,tt}^U)^3 m_b y_t (\Theta_5(y_t) z_A - \Theta_1(z_A, y_t))}{32\pi^2 m_{A^0}^2 m_t \Theta_1(z_A, y_t) \Theta_5(y_t)}, \\ C_{Q_2}^{A^0}((\bar{\xi}_{N,tt}^U)^2) &= \frac{\bar{\xi}_{N,\tau\tau}^D (\bar{\xi}_{N,tt}^U)^2 \bar{\xi}_{N,bb}^D}{32\pi^2 m_{A^0}^2} \left(\frac{1}{\Theta_1(z_A, y_t) \Theta_1(z_A, y_t) \Theta_5(y_t)} \right) \\ &\quad \cdot (y_t (\Theta_1(z_A, y_t) - \Theta_5(y_t) (xy + z_A)) - 2\Theta_1(z_A, y_t) \Theta_5(y_t) \ln[\frac{z_A \Theta_5(y_t)}{\Theta_1(z_A, y_t)}]) \\ C_{Q_2}^{A^0}(\bar{\xi}_{N,tt}^U) &= \frac{g^2 \bar{\xi}_{N,\tau\tau}^D \bar{\xi}_{N,tt}^U m_b x_t}{64\pi^2 m_{A^0}^2 m_t} \left(\frac{2}{\Theta_5(x_t)} - \frac{xy x_t + 2z_A}{\Theta_1(z_A, x_t)} - 2 \ln[\frac{z_A \Theta_5(x_t)}{\Theta_1(z_A, x_t)}] \right. \\ &\quad - xy x_t y_t \frac{(x-1)x_t(y_t/z_A - 1) - (1+x)y_t}{(\Theta_6 - (x-y)(x_t - y_t))(\Theta_3(z_A) + (x-y)(x_t - y_t)z_A)} \\ &\quad \left. - \frac{x(y_t + x_t(1 - y_t/z_A)) - 2y_t}{\Theta_6 \Theta_3(z_A)} \right) \\ C_{Q_2}^{A^0}(\bar{\xi}_{N,bb}^D) &= \frac{g^2 \bar{\xi}_{N,\tau\tau}^D \bar{\xi}_{N,bb}^D}{64\pi^2 m_{A^0}^2} \left(1 - \frac{x_t^2 y_t + 2y(x-1)x_t y_t - z_A(x_t^2 + \Theta_6)}{\Theta_3(z_A)} \right. \\ &\quad \left. + \frac{x_t^2(1 - y_t/z_A)}{\Theta_6} + 2 \ln[\frac{z_A \Theta_6}{\Theta_2(z_A, x)}] \right) \\ C_{Q_1}^{H^0}((\bar{\xi}_{N,tt}^U)^2) &= \frac{g^2 (\bar{\xi}_{N,tt}^U)^2 m_b m_\tau}{64\pi^2 m_{H^0}^2 m_t^2} \left(\frac{x_t(1-2y)y_t}{\Theta_5(y_t)} + \frac{(-1+2\cos^2\theta_W)(-1+x+y)y_t}{\cos^2\theta_W \Theta_4(y_t)} \right. \\ &\quad \left. + \frac{z_H(\Theta_1(z_H, y_t)xy_t + \cos^2\theta_W(-2x^2(-1+x_t)yy_t^2 + xx_tyy_t^2 - \Theta_8z_H))}{\cos^2\theta_W \Theta_1(z_H, y_t) \Theta_7} \right), \\ C_{Q_1}^{H^0}(\bar{\xi}_{N,tt}^U) &= \frac{g^2 \bar{\xi}_{N,tt}^U \bar{\xi}_{N,bb}^D m_\tau}{64\pi^2 m_{H^0}^2 m_t} \left(\frac{(-1+2\cos^2\theta_W)y_t}{\cos^2\theta_W \Theta_4(y_t)} - \frac{x_t y_t}{\Theta_5(y_t)} + \frac{x_t y_t (xy - z_H)}{\Theta_1(z_H, y_t)} \right. \\ &\quad \left. + \frac{(-1+2\cos^2\theta_W)y_t z_H}{\cos^2\theta_W \Theta_7} - 2x_t \ln \left[\frac{\Theta_5(y_t) z_H}{\Theta_1(z_H, y_t)} \right] \right), \end{aligned} \quad (\text{C.4})$$

$$\begin{aligned}
C_{Q_1}^{H^0}(g^4) = & -\frac{g^4 m_b m_\tau x_t}{128\pi^2 m_{H^0}^2 m_t^2} \left(-1 + \frac{(-1+2x)x_t}{\Theta_5(x_t) + y(1-x_t)} + \frac{2x_t(-1+(2+x_t)y)}{\Theta_5(x_t)} \right. \\
& - \frac{4\cos^2\theta_W(-1+x+y) + x_t(x+y)}{\cos^2\theta_W\Theta_4(x_t)} + \frac{x_t(x(x_t(y-2z_H)-4z_H)+2z_H)}{\Theta_1(z_H, x_t)} \\
& + \frac{y_t((-1+x)x_tz_H + \cos^2\theta_W((3x-y)z_H + x_t(2y(x-1)-z_H(2-3x-y))))}{\cos^2\theta_W(\Theta_3(z_H) + x(x_t-y_t)z_H)} \\
& \left. + 2(x_t \ln \left[\frac{\Theta_5(x_t)z_H}{\Theta_1(z_H, x_t)} \right] + \ln \left[\frac{x(y_t-x_t)z_H - \Theta_3(z_H)}{(\Theta_5(x_t) + y(1-x_t)y_t)z_H} \right]) \right),
\end{aligned}$$

$$C_{Q_1}^{h_0}((\bar{\xi}_{N,tt}^U)^3) = -\frac{\bar{\xi}_{N,\tau\tau}^D(\bar{\xi}_{N,tt}^U)^3 m_b y_t}{32\pi^2 m_{h^0}^2 m_t \Theta_1(z_h, y_t) \Theta_5(y_t)} \left(\Theta_1(z_h, y_t)(2y-1) + \Theta_5(y_t)(2x-1)z_h \right)$$

$$\begin{aligned}
C_{Q_1}^{h_0}((\bar{\xi}_{N,tt}^U)^2) = & \frac{\bar{\xi}_{N,\tau\tau}^D(\bar{\xi}_{N,tt}^U)^2}{32\pi^2 m_{h^0}^2} \left(\frac{(\Theta_5(y_t)z_h(y_t-1)(x+y-1) - \Theta_1(z_h, y_t)(\Theta_5(y_t) + y_t))}{\Theta_1(z_h)\Theta_5(y_t)} \right. \\
& \left. - 2 \ln \left[\frac{z_h\Theta_5(y_t)}{\Theta_1(z_h)} \right] \right)
\end{aligned}$$

$$\begin{aligned}
C_{Q_1}^{h^0}(\bar{\xi}_{N,tt}^U) = & -\frac{g^2 \bar{\xi}_{N,\tau\tau}^D \bar{\xi}_{N,tt}^U m_b x_t}{64\pi^2 m_{h^0}^2 m_t} \left(\frac{2(-1+(2+x_t)y)}{\Theta_5(x_t)} - \frac{x_t(x-1)(y_t-z_h)}{\Theta_2'(z_h)} + 2 \ln \left[\frac{z_h\Theta_5(x_t)}{\Theta_1(z_h, x_t)} \right] \right. \\
& + \frac{x(x_t(y-2z_h)-4z_h)+2z_h}{\Theta_1(z_h, x_t)} - \frac{(1+x)y_t z_h}{x y x_t y_t + z_h((x-y)(x_t-y_t) - \Theta_6)} \\
& \left. + \frac{\Theta_9 + y_t z_h((x-y)(x_t-y_t) - \Theta_6)(2x-1)}{z_h\Theta_6(\Theta_6 - (x-y)(x_t-y_t))} + \frac{x(y_t z_h + x_t(z_h-y_t)) - 2y_t z_h}{\Theta_2(z_h)} \right),
\end{aligned}$$

$$\begin{aligned}
C_{Q_1}^{h^0}(\bar{\xi}_{N,bb}^D) = & -\frac{g^2 \bar{\xi}_{N,\tau\tau}^D \bar{\xi}_{N,bb}^D}{64\pi^2 m_{h^0}^2} \left(\frac{y x_t y_t (x x_t^2 (y_t - z_h) + \Theta_6 z_h (x - 2))}{z_h \Theta_2(z_h) \Theta_6} + 2 \ln \left[\frac{\Theta_6}{x_t y_t} \right] \right. \\
& \left. + 2 \ln \left[\frac{x_t y_t z_h}{\Theta_2(z_h)} \right] \right)
\end{aligned}$$

where

$$\begin{aligned}
\Theta_1(\omega, \lambda) &= -(-1+y-y\lambda)\omega - x(y\lambda + \omega - \omega\lambda) \\
\Theta_2(\omega) &= (x_t + y(1-x_t))y_t\omega - x x_t(y y_t + (y_t-1)\omega) \\
\Theta_2'(\omega) &= \Theta_2(\omega, x_t \leftrightarrow y_t)
\end{aligned}$$

$$\begin{aligned}
\Theta_3(\omega) &= (x_t(-1+y) - y)y_t\omega + xx_t(yy_t + \omega(-1+y_t)) \\
\Theta_4(\omega) &= 1 - x + x\omega \\
\Theta_5(\lambda) &= x + \lambda(1-x) \\
\Theta_6 &= (x_t + y(1-x_t))y_t + xx_t(1-y_t) \\
\Theta_7 &= (y(y_t-1) - y_t)z_H + x(yy_t + (y_t-1)z_H) \\
\Theta_8 &= y_t(2x^2(1+x_t)(y_t-1) + x_t(y(1-y_t) + y_t) + x(2(1-y+y_t) \\
&\quad + x_t(1-2y(1-y_t) - 3y_t))) \\
\Theta_9 &= -x_t^2(-1+x+y)(-y_t + x(2y_t-1))(y_t - z_h) - x_ty_tz_h(x(1+2x) - 2y) \\
&\quad + y_t^2(x_t(x^2 - y(1-x)) + (1+x)(x-y)z_h)
\end{aligned} \tag{C.5}$$

and

$$x_t = \frac{m_t^2}{m_W^2}, \quad y_t = \frac{m_t^2}{m_{H^\pm}}, \quad z_H = \frac{m_t^2}{m_{H^0}^2}, \quad z_h = \frac{m_t^2}{m_{h^0}^2}, \quad z_A = \frac{m_t^2}{m_{A^0}^2}.$$

The explicit forms of the functions $F_{1(2)}(y_t)$, $G_{1(2)}(y_t)$, $H_1(y_t)$ and $L_1(y_t)$ in Eq.(C.2) are given as

$$\begin{aligned}
F_1(y_t) &= \frac{y_t(7-5y_t-8y_t^2)}{72(y_t-1)^3} + \frac{y_t^2(3y_t-2)}{12(y_t-1)^4} \ln y_t, \\
F_2(y_t) &= \frac{y_t(5y_t-3)}{12(y_t-1)^2} + \frac{y_t(-3y_t+2)}{6(y_t-1)^3} \ln y_t, \\
G_1(y_t) &= \frac{y_t(-y_t^2+5y_t+2)}{24(y_t-1)^3} + \frac{-y_t^2}{4(y_t-1)^4} \ln y_t, \\
G_2(y_t) &= \frac{y_t(y_t-3)}{4(y_t-1)^2} + \frac{y_t}{2(y_t-1)^3} \ln y_t, \\
H_1(y_t) &= \frac{1-4\sin^2\theta_W}{\sin^2\theta_W} \frac{xy_t}{8} \left[\frac{1}{y_t-1} - \frac{1}{(y_t-1)^2} \ln y_t \right] \\
&\quad - y_t \left[\frac{47y_t^2-79y_t+38}{108(y_t-1)^3} - \frac{3y_t^3-6y_t+4}{18(y_t-1)^4} \ln y_t \right], \\
L_1(y_t) &= \frac{1}{\sin^2\theta_W} \frac{xy_t}{8} \left[-\frac{1}{y_t-1} + \frac{1}{(y_t-1)^2} \ln y_t \right].
\end{aligned} \tag{C.6}$$

Finally, the initial values of the coefficients in the model III are

$$\begin{aligned}
C_i^{2HDM}(m_W) &= C_i^{SM}(m_W) + C_i^H(m_W), \\
C_{Q_1}^{2HDM}(m_W) &= \int_0^1 dx \int_0^{1-x} dy (C_{Q_1}^{H^0}((\bar{\xi}_{N,tt}^U)^2) + C_{Q_1}^{H^0}(\bar{\xi}_{N,tt}^U) + C_{Q_1}^{H^0}(g^4) + C_{Q_1}^{h^0}((\bar{\xi}_{N,tt}^U)^3)
\end{aligned}$$

$$\begin{aligned}
& + C_{Q_1}^{h^0}((\bar{\xi}_{N,tt}^U)^2) + C_{Q_1}^{h^0}(\bar{\xi}_{N,tt}^U) + C_{Q_1}^{h^0}(\bar{\xi}_{N,bb}^D)), \\
C_{Q_2}^{2HDM}(m_W) & = \int_0^1 dx \int_0^{1-x} dy (C_{Q_2}^{A^0}((\bar{\xi}_{N,tt}^U)^3) + C_{Q_2}^{A^0}((\bar{\xi}_{N,tt}^U)^2) + C_{Q_2}^{A^0}(\bar{\xi}_{N,tt}^U) + C_{Q_2}^{A^0}(\bar{\xi}_{N,bb}^D)) \\
C_{Q_3}^{2HDM}(m_W) & = \frac{m_b}{m_\tau \sin^2 \theta_W} (C_{Q_1}^{2HDM}(m_W) + C_{Q_2}^{2HDM}(m_W)) \\
C_{Q_4}^{2HDM}(m_W) & = \frac{m_b}{m_\tau \sin^2 \theta_W} (C_{Q_1}^{2HDM}(m_W) - C_{Q_2}^{2HDM}(m_W)) \\
C_{Q_i}^{2HDM}(m_W) & = 0, \quad i = 5, \dots, 10. \tag{C.7}
\end{aligned}$$

Here, we present C_{Q_1} and C_{Q_2} in terms of the Feynman parameters x and y since the integrated results are extremely large. Using these initial values, we can calculate the coefficients $C_i^{2HDM}(\mu)$ and $C_{Q_i}^{2HDM}(\mu)$ at any lower scale in the effective theory with five quarks, namely u, c, d, s, b similar to the SM case [19, 23, 25, 26].

The Wilson coefficients playing the essential role in this process are $C_7^{2HDM}(\mu)$, $C_9^{2HDM}(\mu)$, $C_{10}^{2HDM}(\mu)$, $C_{Q_1}^{2HDM}(\mu)$ and $C_{Q_2}^{2HDM}(\mu)$. For completeness, in the following we give their explicit expressions,

$$C_7^{eff}(\mu) = C_7^{2HDM}(\mu) + Q_d (C_5^{2HDM}(\mu) + N_c C_6^{2HDM}(\mu)) ,$$

where the LO QCD corrected Wilson coefficient $C_7^{LO,2HDM}(\mu)$ is given by

$$\begin{aligned}
C_7^{LO,2HDM}(\mu) & = \eta^{16/23} C_7^{2HDM}(m_W) + (8/3)(\eta^{14/23} - \eta^{16/23}) C_8^{2HDM}(m_W) \\
& + C_2^{2HDM}(m_W) \sum_{i=1}^8 h_i \eta^{a_i} , \tag{C.8}
\end{aligned}$$

and $\eta = \alpha_s(m_W)/\alpha_s(\mu)$, h_i and a_i are the numbers which appear during the evaluation [26].

$C_9^{eff}(\mu)$ contains a perturbative part and a part coming from LD effects due to conversion of the real $\bar{c}c$ into lepton pair $\ell^+ \ell^-$:

$$C_9^{eff}(\mu) = C_9^{pert}(\mu) + Y_{reson}(s) , \tag{C.9}$$

where

$$\begin{aligned}
C_9^{pert}(\mu) & = C_9^{2HDM}(\mu) \\
& + h(z, s) (3C_1(\mu) + C_2(\mu) + 3C_3(\mu) + C_4(\mu) + 3C_5(\mu) + C_6(\mu)) \\
& - \frac{1}{2} h(1, s) (4C_3(\mu) + 4C_4(\mu) + 3C_5(\mu) + C_6(\mu)) \\
& - \frac{1}{2} h(0, s) (C_3(\mu) + 3C_4(\mu)) + \frac{2}{9} (3C_3(\mu) + C_4(\mu) + 3C_5(\mu) + C_6(\mu)) , \tag{C.10}
\end{aligned}$$

and

$$Y_{reson}(s) = -\frac{3}{\alpha_{em}^2} \kappa \sum_{V_i=\psi_i} \frac{\pi \Gamma(V_i \rightarrow \ell^+ \ell^-) m_{V_i}}{q^2 - m_{V_i}^2 + i m_{V_i} \Gamma_{V_i}} (3C_1(\mu) + C_2(\mu) + 3C_3(\mu) + C_4(\mu) + 3C_5(\mu) + C_6(\mu)) \quad (C.11)$$

In eq.(C.9), the functions $h(u, s)$ are given by

$$h(u, s) = -\frac{8}{9} \ln \frac{m_b}{\mu} - \frac{8}{9} \ln u + \frac{8}{27} + \frac{4}{9} x - \frac{2}{9} (2+x) |1-x|^{1/2} \begin{cases} \left(\ln \left| \frac{\sqrt{1-x}+1}{\sqrt{1-x}-1} \right| - i\pi \right), & \text{for } x \equiv \frac{4u^2}{s} < 1 \\ 2 \arctan \frac{1}{\sqrt{x-1}}, & \text{for } x \equiv \frac{4u^2}{s} > 1, \end{cases} \quad (C.12)$$

$$h(0, s) = \frac{8}{27} - \frac{8}{9} \ln \frac{m_b}{\mu} - \frac{4}{9} \ln s + \frac{4}{9} i\pi, \quad (C.13)$$

with $u = \frac{m_c}{m_b}$. The phenomenological parameter κ in eq. (C.11) is taken as 2.3. In Eqs. (37) and (C.11), the contributions of the coefficients $C_1(\mu), \dots, C_6(\mu)$ are due to the operator mixing.

Finally, the Wilson coefficients $C_{Q_1}(\mu)$ and $C_{Q_2}(\mu)$ are given by [15]

$$C_{Q_i}(\mu) = \eta^{-12/23} C_{Q_i}(m_W), \quad i = 1, 2. \quad (C.14)$$

Appendix D

Some functions appearing in the expressions

We parametrize the functions A_1, A_2, B_1, B_2, F_1 and F_2 in Eqs. (4) and (6) as

$$\begin{aligned} A_1 &= A_1^{(1)} + i A_1^{(2)} + \bar{\xi}_{N,bb}^D A_1^{(3)} \\ A_2 &= A_2^{(1)} + i A_2^{(2)} + \bar{\xi}_{N,bb}^D A_2^{(3)} \\ B_1 &= C_{10} g, \\ B_2 &= C_{10} f, \\ F &= 2m_\tau C_{10} + \frac{m_B^2}{m_b^2} \left(F^{(1)} + \bar{\xi}_{N,bb}^D F^{(2)} \right), \\ F_1 &= \frac{m_B^2}{m_b^2} \left(F_1^{(1)} + \bar{\xi}_{N,bb}^D F_1^{(2)} \right), \end{aligned} \quad (D.1)$$

with

$$A_1^{(1)} = g \operatorname{Re}(C_9^{eff}) - \frac{2m_b}{q^2} g_1 C_7^{eff} \Big|_{\bar{\xi}_{N,bb}^D \rightarrow 0},$$

$$\begin{aligned}
A_1^{(2)} &= g \operatorname{Im}(C_9^{eff}) , \\
A_1^{(3)} &= -\frac{2m_b}{q^2} g_1 \frac{1}{m_b m_t} \bar{\xi}_{N,tt}^U (\eta^{\frac{16}{23}} K_2(y_t) + \frac{8}{3} (\eta^{\frac{14}{23}} - \eta^{\frac{16}{23}}) G_2(y_t)) , \\
A_2^{(1)} &= A_1^{(1)}(g \rightarrow f; g_1 \rightarrow f_1) , \\
A_2^{(2)} &= A_1^{(2)}(g \rightarrow f) , \\
A_2^{(3)} &= A_1^{(3)}(g_1 \rightarrow f_1) , \\
F_1^{(1)} &= \eta^{-12/23} \int_0^1 dx \int_0^{1-x} dy [C_{Q_1}^{H_0}((\bar{\xi}_{N,tt}^U)^2) + C_{Q_1}^{H_0}(\bar{\xi}_{N,tt}^U) \\
&\quad + C_{Q_1}^{H_0}(g^4) + C_{Q_1}^{h_0}((\bar{\xi}_{N,tt}^U)^3) + C_{Q_1}^{h_0}((\bar{\xi}_{N,tt}^U)^2) + C_{Q_1}^{h_0}(\bar{\xi}_{N,tt}^U)] , \\
F_1^{(2)} &= \frac{\eta^{-12/23}}{\bar{\xi}_{N,bb}^D} \int_0^1 dx \int_0^{1-x} dy C_{Q_1}^{h_0}(\bar{\xi}_{N,bb}^D) , \\
F^{(1)} &= \eta^{-12/23} \int_0^1 dx \int_0^{1-x} dy [C_{Q_2}^{A_0}((\bar{\xi}_{N,tt}^U)^3) + C_{Q_2}^{A_0}((\bar{\xi}_{N,tt}^U)^2) + C_{Q_2}^{A_0}(\bar{\xi}_{N,tt}^U)] , \\
F^{(2)} &= \frac{\eta^{-12/23}}{\bar{\xi}_{N,bb}^D} \int_0^1 dx \int_0^{1-x} dy C_{Q_2}^{A_0}(\bar{\xi}_{N,bb}^D) . \tag{D.2}
\end{aligned}$$

REFERENCES

- [1] J. L. Hewett, in Proc. of the 21st Annual SLAC Summer Institute, ed. L. De Porcel and C. Dunwoode, SLAC-PUB-6521 (1994)
- [2] R. Ammar, *et all.*, CLEO Collaboration, *Phys. Rev. Lett.* **71** (1993) 674; M. S. Alam, *et all.*, CLEO Collaboration, *Phys. Rev. Lett.* **74** (1995) 2885.
- [3] M. S. Alam, *et all.*, CLEO Collaboration, in ICHEP98 Conference 1998; ALEPH Collaboration, R. Barate *et all.*, *Phys. Lett.* **B429** (1998) 169.
- [4] G. Eilam, C.-D. Lü and D.-X. Zhang, *Phys. Lett.* **B 391** (1997) 461.
- [5] T. M. Aliev, A. Özpineci, and M. Savci, *Phys. Rev. D* **55** (1997) 7059.
- [6] T. M. Aliev, N. K. Pak, and M. Savci, *Phys. Lett.* **B 424** (1998) 175.
- [7] Z. Xiong and J. M. Yang, *hep-ph/0105260*
- [8] E. O. Iltan and G. Turan, *Phys. Rev. D* **61** (2000) 034010.
- [9] T. M. Aliev, A. Özpineci and M. Savci, *Phys. Lett.* **B 520** (2001) 69.
- [10] G. Erkol and G. Turan, *hep-ph/0110017*
- [11] L3 Collaboration, *Phys. Lett.* **B 503** (2001) 21.
- [12] E. O. Iltan, *Phys. Rev. D* **60** (1999) 034023.
- [13] E. O. Iltan, *Phys. Rev. D* **61** (1999) 054001.
- [14] E. O. Iltan, G. Turan and I. Turan, *hep-ph/0106136*.
- [15] Y. B. Dai, C. S. Huang and H. W. Huang, *Phys. Lett.* **B390** (1997) 257, erratum **B513** (2001) 429 ; C. S. Huang, L. Wei, Q. S. Yan and S. H. Zhu, *Phys. Rev. D* **63** (2001) 114021.
- [16] C. Bobeth, T. Ewerth, F. Krüger and J. Urban, *Phys. Rev. D* **64** (2001) 074014.
- [17] G. Eilam, I. Halperin and R. R. Mendel, *Phys. Lett.* **B 361** (1995) 137.
- [18] G. Buchalla and A. J. Buras, *Nucl. Phys.* **B400** (1993) 225.
- [19] T. M. Aliev, and E. Iltan, *Phys. Rev. D* **58** (1998) 095014.
- [20] T. M. Aliev, E. O. Iltan, *J. Phys. G. Nucl. Part. Phys.* **25** (1999) 989.
- [21] D. Atwood, L. Reina and A. Soni, *Phys. Rev. D* **55** (1997) 3156.
- [22] B. Grinstein, R. Springer, and M. Wise, *Nuc. Phys.* **B339** (1990) 269; R. Grigjanis, P.J. O'Donnell, M. Sutherland and H. Navelet, *Phys. Lett.* **B213** (1988) 355; *Phys. Lett.* **B286** (1992) E, 413; G. Cella, G. Curci, G. Ricciardi and A. Viceré, *Phys. Lett.* **B325** (1994) 227, *Nucl. Phys.* **B431** (1994) 417.
- [23] M. Misiak, *Nucl. Phys.* **B393** (1993) 23, Erratum **B439** (1995) 461.
- [24] E. Iltan and G. Turan, *Phys. Rev. D* **63** (2001) 115007.
- [25] C. S. Huang, *Nucl. Phys. Proc. Suppl.* **93** (2001) 73
- [26] A. J. Buras and M. Münz, *Phys. Rev. D* **52** (1995) 186.

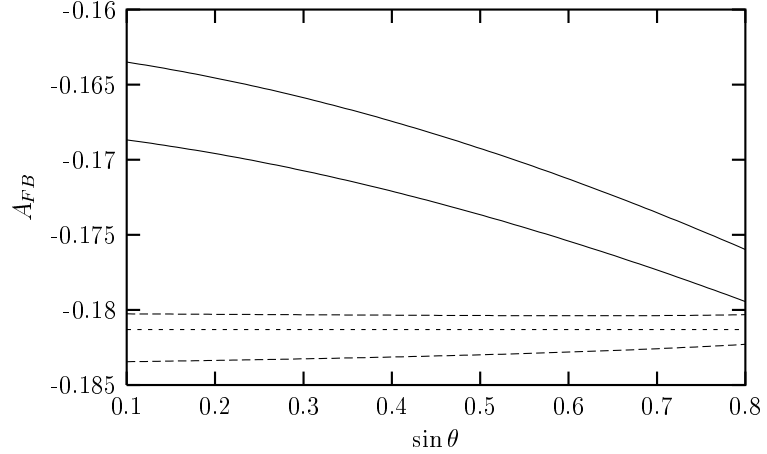


Fig. 1. A_{FB} as a function of $\sin \theta$ for $\bar{\xi}_{N,bb}^D = 40 m_b$ and $|r_{tb}| < 1$ without NHB effects. Here A_{FB} is restricted in the region between solid (dashed) curves for $C_7^{eff} > 0$ ($C_7^{eff} < 0$). Dashed straight line represents the SM prediction.

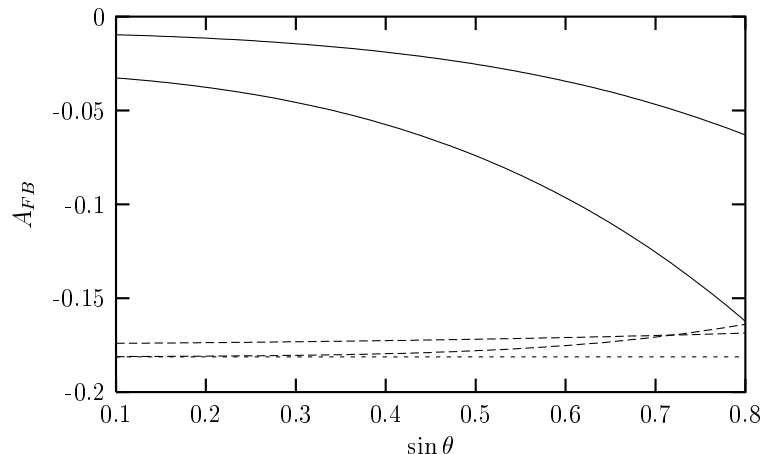


Fig. 2. The same as Fig. 1, but including NHB effects with $\bar{\xi}_{N,\tau\tau}^D = 10 m_\tau$.

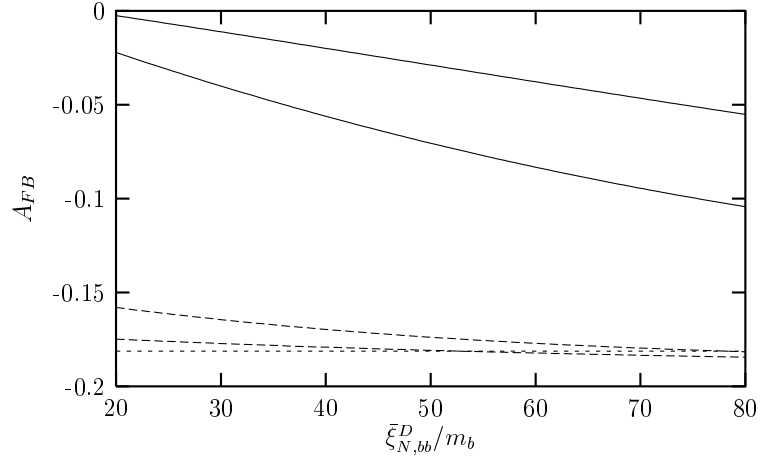


Fig. 3. A_{FB} as a function of $\bar{\xi}_{N,bb}^D/m_b$ for $\bar{\xi}_{N,\tau\tau}^D = 10 m_\tau$, $\sin \theta = 0.5$ and $|r_{tb}| < 1$. Here A_{FB} is restricted in the region between solid (dashed) curves for $C_7^{eff} > 0$ ($C_7^{eff} < 0$). Dashed straight line represents the SM prediction.

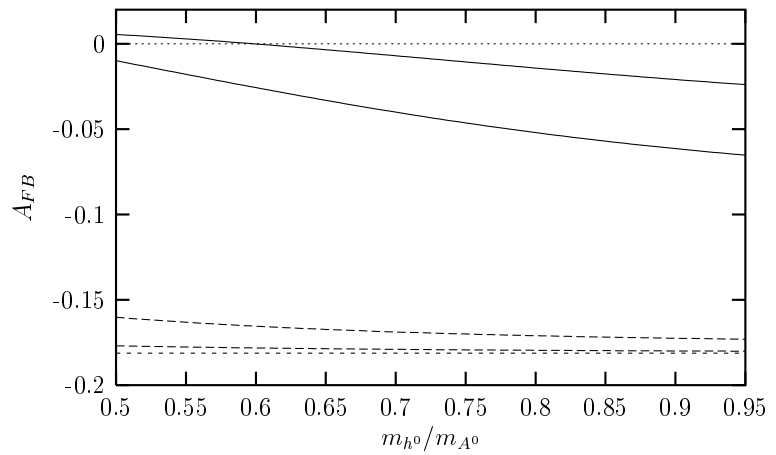


Fig. 4. The same as Fig. 3, but as a function of m_{h^0}/m_{A^0} .

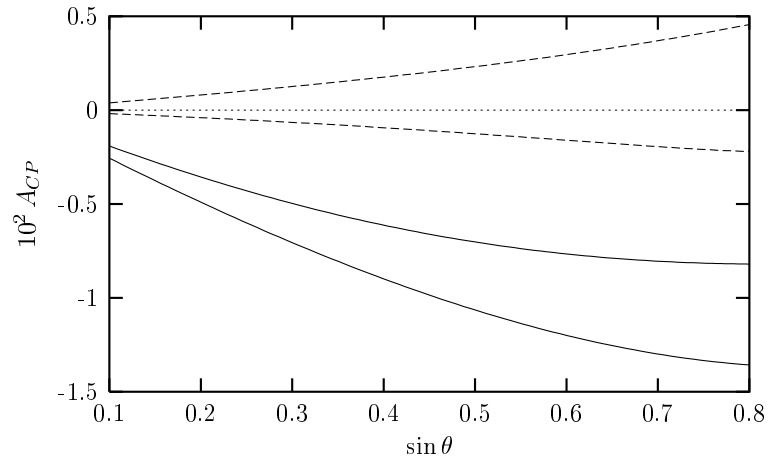


Fig. 5. The same as Fig. 1, but for A_{CP} .

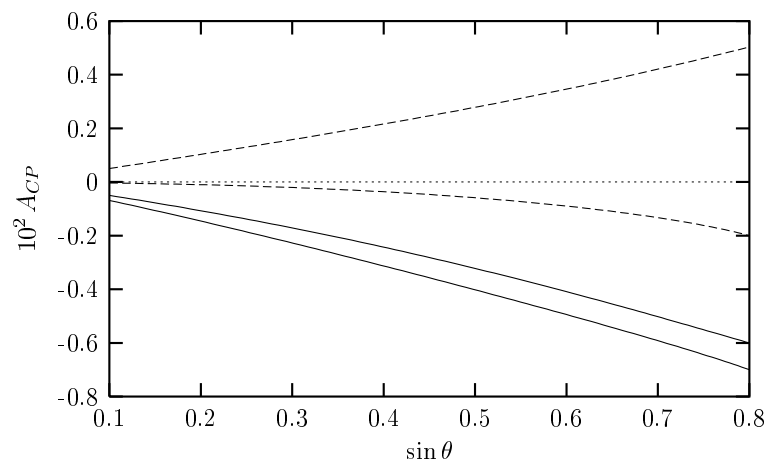


Fig. 6. The same as Fig. 2, but for A_{CP} .

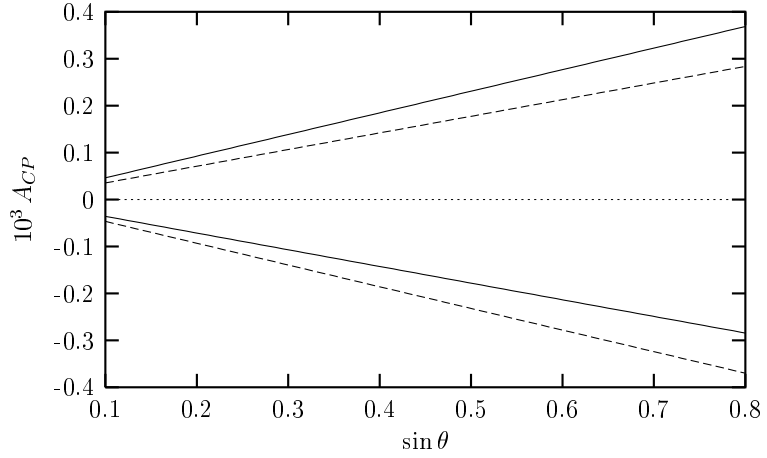


Fig. 7. A_{CP} as a function of $\sin \theta$ for $\bar{\xi}_{N,bb}^D = 0.1 m_b$ and $r_{tb} > 1$ without NHB effects. Here A_{CP} is restricted in the region between solid (dashed) curves for $C_7^{eff} > 0$ ($C_7^{eff} < 0$).

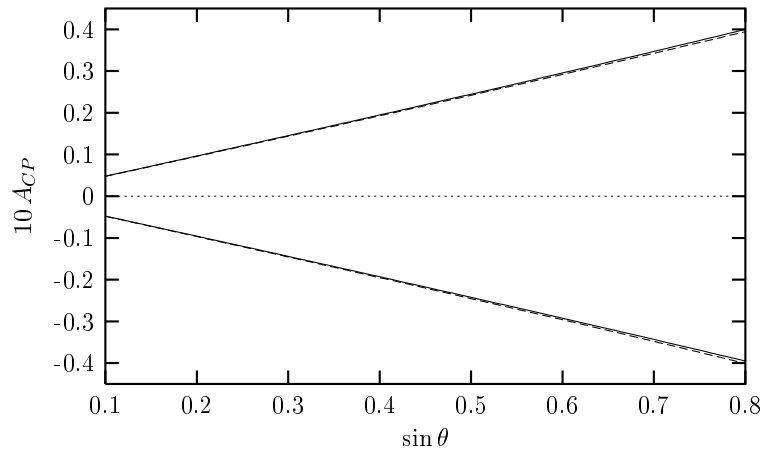


Fig. 8. The same as Fig. 7, but including NHB effects with $\bar{\xi}_{N,\tau\tau}^D = m_\tau$.

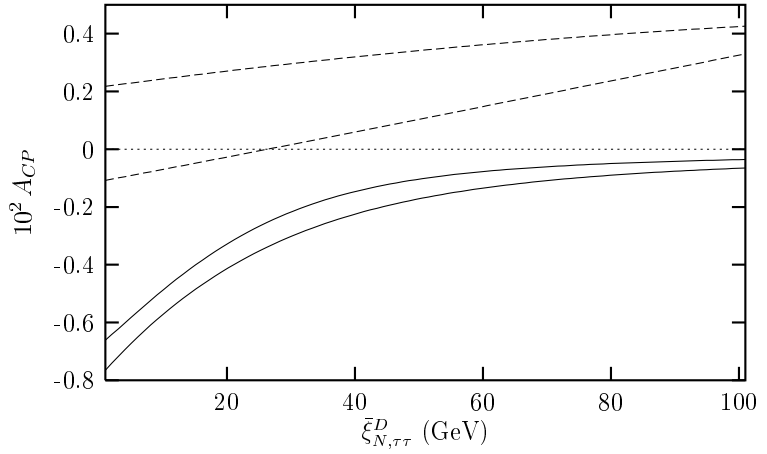


Fig. 9. A_{CP} as a function of $\bar{\xi}_{N,\tau\tau}^D$ for $\bar{\xi}_{N,bb}^D = 40 m_b$, $\sin \theta = 0.5$ and $|r_{tb}| < 1$. Here A_{CP} is restricted in the region between solid (dashed) curves for $C_7^{eff} > 0$ ($C_7^{eff} < 0$).

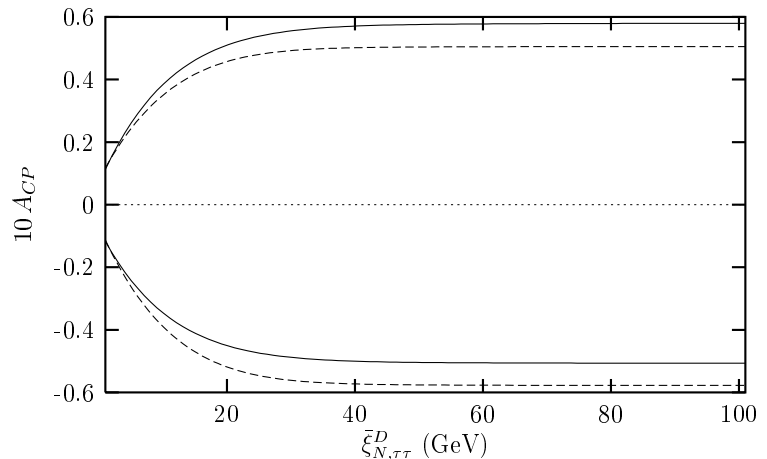


Fig. 10. The same as Fig. 9, but for $r_{tb} > 1$ with $\bar{\xi}_{N,bb}^D = 0.1 m_b$.

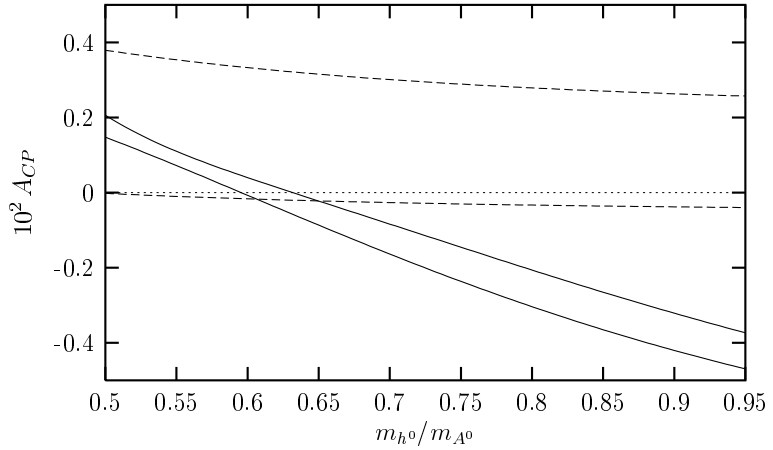


Fig. 11. A_{CP} as a function of m_{h^0}/m_{A^0} for $\bar{\xi}_{N,\tau\tau}^D = 10 m_\tau$, $\bar{\xi}_{N,bb}^D = 40 m_b$, $\sin \theta = 0.5$ and $|r_{tb}| < 1$. Here A_{CP} is restricted in the region between solid (dashed) curves for $C_7^{eff} > 0$ ($C_7^{eff} < 0$).

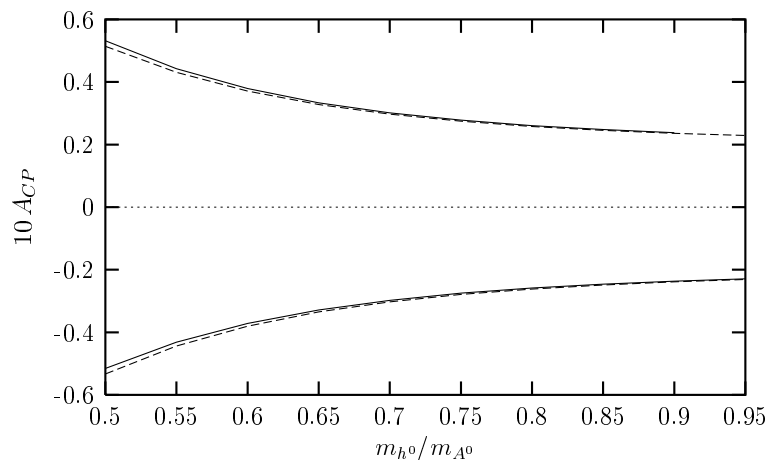


Fig. 12. The same as Fig. 11, but for $r_{tb} > 1$ with $\bar{\xi}_{N,\tau\tau}^D = m_\tau$ and $\bar{\xi}_{N,bb}^D = 0.1 m_b$.

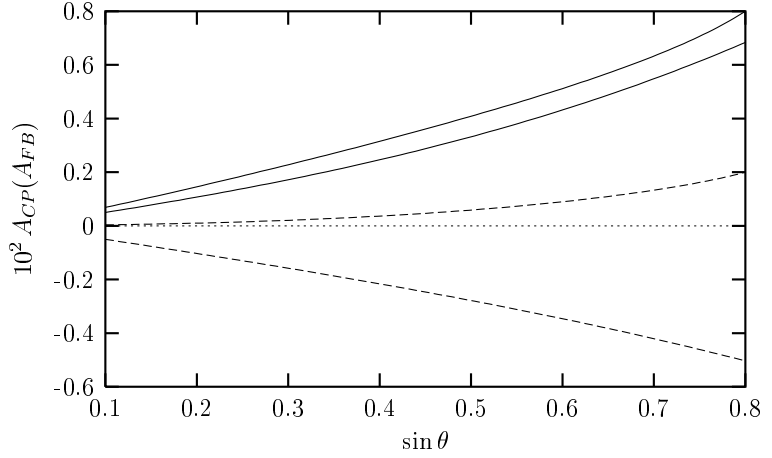


Fig. 13. $A_{CP}(A_{FB})$ as a function of $\sin \theta$ for $\bar{\xi}_{N,\tau\tau}^D = 10 m_\tau$, $\bar{\xi}_{N,bb}^D = 40 m_b$ and $|r_{tb}| < 1$. Here $A_{CP}(A_{FB})$ is restricted in the region between solid (dashed) curves for $C_7^{eff} > 0$ ($C_7^{eff} < 0$).

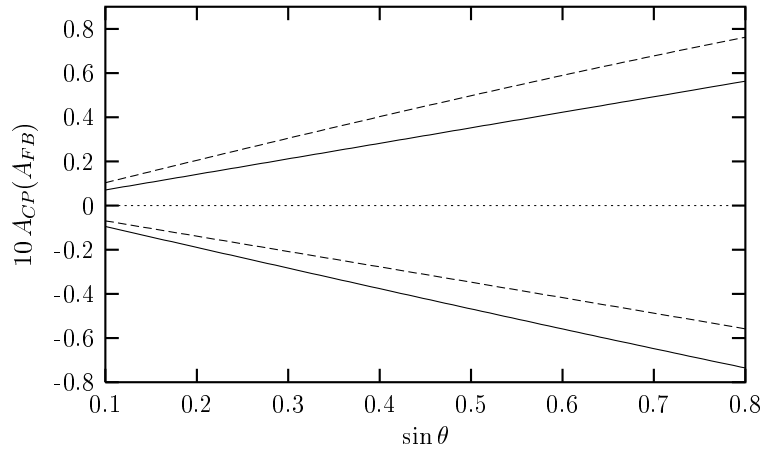


Fig. 14. The same as Fig. 13, but for $r_{tb} > 1$ with $\bar{\xi}_{N,\tau\tau}^D = m_\tau$ and $\bar{\xi}_{N,bb}^D = 0.1 m_b$.

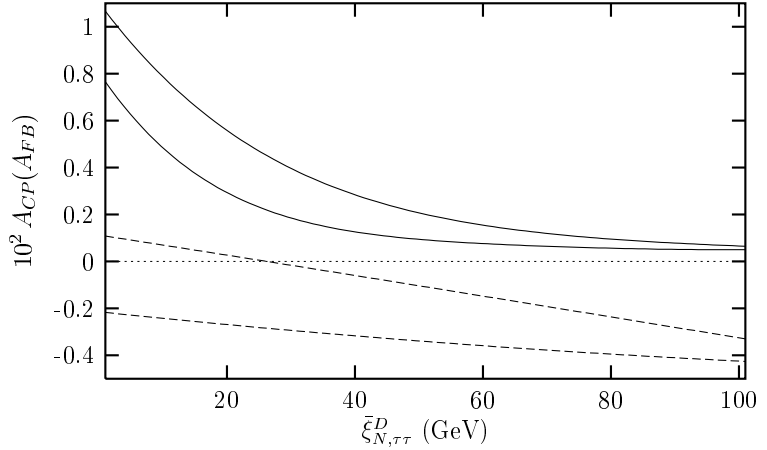


Fig. 15. $A_{CP}(A_{FB})$ as a function of $\bar{\xi}_{N,\tau\tau}^D$ for $\bar{\xi}_{N,bb}^D = 40\text{ }m_b$, $\sin \theta = 0.5$ and $|r_{tb}| < 1$. Here $A_{CP}(A_{FB})$ is restricted in the region between solid (dashed) curves for $C_7^{eff} > 0$ ($C_7^{eff} < 0$).

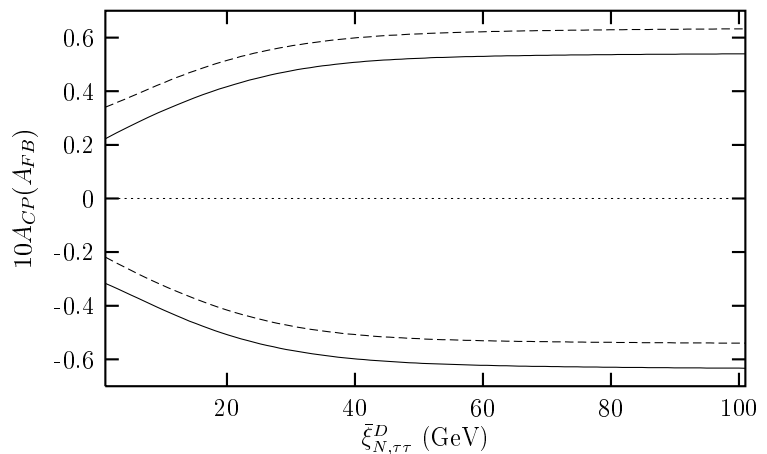


Fig. 16. The same as Fig. 15, but for $r_{tb} > 1$ with $\bar{\xi}_{N,bb}^D = 0.1\text{ }m_b$.

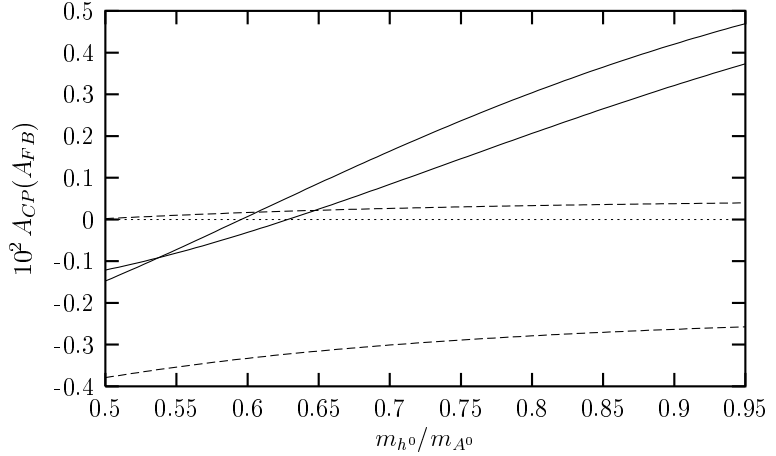


Fig. 17. $A_{CP}(A_{FB})$ as a function of m_{h^0}/m_{A^0} for $\bar{\xi}_{N,\tau\tau}^D = 10 m_\tau$, $\bar{\xi}_{N,bb}^D = 40 m_b$, $\sin \theta = 0.5$ and $|r_{tb}| < 1$. Here $A_{CP}(A_{FB})$ is restricted in the region between solid (dashed) curves for $C_7^{eff} > 0$ ($C_7^{eff} < 0$).

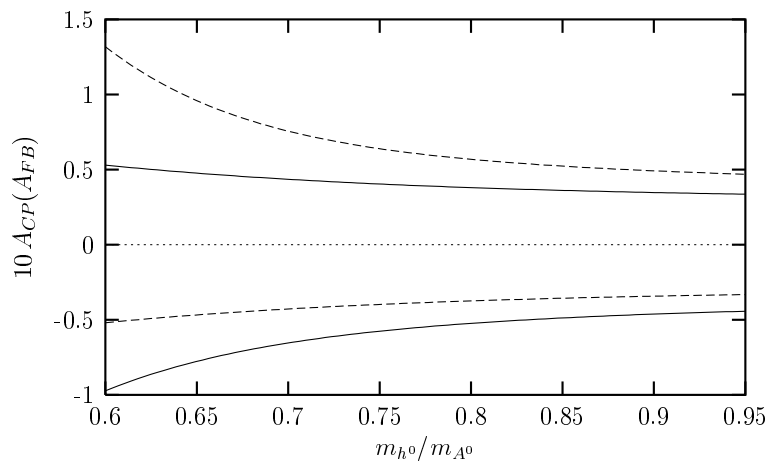


Fig. 18. The same as Fig. 17, but for $r_{tb} > 1$ with $\bar{\xi}_{N,\tau\tau}^D = m_\tau$ and $\bar{\xi}_{N,bb}^D = 0.1 m_b$.